

HOW RAPIDLY DO SUPERMASSIVE BLACK HOLE “SEEDS” GROW AT EARLY TIMES?

FEDERICO I. PELUPESSY¹, TIZIANA DI MATTEO¹, BENEDETTA CIARDI²

Draft version April 18, 2007

ABSTRACT

We investigate the physical conditions for the growth of intermediate mass seed black holes assumed to have formed from remnants of the first generation of massive stars. We follow the collapse of high- σ halos with $T_{vir} > 10^4$ K using cosmological, smooth-particle hydrodynamic (SPH) simulations in the standard Λ CDM model. During collapse of the parent halo the seed holes are incorporated through mergers into larger systems and accrete mass from the surrounding gas. We include a self-consistent treatment of star formation, black hole accretion and associated feedback processes. Even under optimistic assumptions for the seed black hole mass and for efficient merger rates, we find that seed holes in halos $M \leq 10^{10} M_{\odot}$ never reach the conditions for critical Eddington growth. Most of the black hole growth in this regime is determined by the initial mass and the merger rates. Critical accretion rates are reached, albeit only after a significant delay, at the time of collapse ($z \sim 7$) for $3-4\sigma$ halos of $M \sim 10^{11} M_{\odot}$. Our results imply $M_{BH} = 5 \times 10^6 M_{\odot} (M_{halo}/10^{11} M_{\odot})^{0.78}$ at the time of collapse. The required conditions of Eddington growth to explain the build-up of supermassive black holes ($\sim 10^9 M_{\odot}$), as implied by Sloan quasars at $z > 6$, are therefore hard to meet in such a scenario. Without a ‘jump-start’ these conditions may be only achieved in extremely rare halos with $M_{halo} > 10^{13}$ that collapsed before $z \sim 6$. The sub-Eddington regime in which black holes accrete at early time implies a small contribution to the reionization by miniquasar but still sufficient to cause appreciable heating of the IGM at $z \lesssim 15 - 18$.

Subject headings: quasars: general — galaxies: formation — galaxies: active — galaxies: evolution — cosmology: theory — hydrodynamics

1. INTRODUCTION

Following the discovery of quasars (Schmidt 1963; Greenstein and Matthews 1963) it was suggested that supermassive black holes ($10^6 - 10^9 M_{\odot}$) lie at the centers of galaxies, and that the quasar activity is fueled by the release of gravitational energy from their accreted matter. The remnants of quasar phases at early times are probably the supermassive black holes (SMBHs) found at the centers of galaxies in our local Universe. Indeed, the properties of SMBHs found at the centers of galaxies today are tightly coupled to those of their host galaxies thus providing strong observational evidence for a close connection between the formation and evolution of galaxies and of their central black holes (Magorrian et al. 1998; Ferrarese and Merritt 2000; Gebhardt et al. 2000). Remarkably, quasars with inferred black hole masses in excess of $10^9 M_{\odot}$ have now been discovered out to $z \sim 6$ (Fan et al. 2003), posing a significant challenge for theoretical models of high-redshift quasar and galaxy formation. The origin, seed mass and the physical conditions for their subsequent growth to supermassive black holes remain uncertain.

The various scenarios that have been proposed for the black hole ‘seed’ progenitors can be broadly grouped into two main ideas. One possible route traces the black hole ‘seeds’ to the remnants of the first generation of PopIII stars. Numerical simulations of the fragmentation of primordial clouds in the standard cold dark matter model suggest that these PopIII, formed of metal-free gas at

$z \sim 20 - 30$, are indeed very massive (Bromm et al. 1999; Abel et al. 2000; Nakamura and Umemura 2001; Yoshida et al. 2003; Gao et al. 2006) and are expected to leave behind a remnant black hole seed in the range of $10 - 10^4 M_{\odot}$. Alternatively, a different mass scale of $10^5 - 10^6 M_{\odot}$ is predicted from models in which seed black holes form directly from the collapse of low angular momentum, dense gas in the center of massive halos with virial temperatures above 10^4 K (Haehnelt and Rees 1993; Umemura et al. 1993; Loeb and Rasio 1994; Eisenstein and Loeb 1995; Bromm and Loeb 2003; Koushiappas et al. 2004; Begelman et al. 2006). Even though the disposal of angular momentum from the gas is a strong constraint in these models, they offer a promising scenario: seed black holes formed in this way have a ‘jump-start’ for their growth into the Sloan quasars.

In the most commonly adopted scenario, in which the first black holes are traced to the first generation of stars, growing the seeds up to $10^9 M_{\odot}$, (as implied by the Sloan quasars at $z \sim 6$) requires an almost continuous accretion of gas at the critical, Eddington rate. If we assume that early black holes grow by accretion at some fraction f of the Eddington rate, then the black hole mass $M_{BH}(z) = M_0 \exp(f \Delta t(z, z_0)/t_s)$, with t_s the Salpeter time and M_0 and z_0 are the formation redshift and mass, while $\Delta t(z, z_0)$ indicates the time between z_0 and redshift z . From this follows that with less than about ~ 800 Myr to $z = 6$ and a Salpeter time of $t_s = 45$ Myr (assuming a radiative efficiency of 10%), the accretion rate should be $f > t_s/\Delta t \log(M_{(z=6)}/M_0) \sim 0.6 - 0.9$ of Eddington, or equivalently an Eddington accretion rate should be sustained at least for $f \sim 60 - 90\%$ of the time to $z = 6$. It is an open question however whether such vigorous Eddington growth can be reached soon enough and

¹ Physics Department, Carnegie Mellon University, 5000 Forbes Avenue, Pittsburgh, PA 15213

² Max-Planck-Institut für Astrophysik, Karl-Schwarzschild-Strasse 1, 85740 Garching bei München, Germany

sustained in the shallow potential at early times. The question of how much mass is accreted and therefore how much energy is liberated by the first miniquasars has also a significant impact for the proposed scenarios of reionization and X-ray heating of the intergalactic medium (IGM) (e.g. Madau et al. 1999; Valageas and Silk 1999; Miralda-Escudé et al. 2000; Oh 2001; Venkatesan et al. 2001; Wyithe and Loeb 2003; Madau et al. 2004; Ricotti and Ostriker 2004; Zaroubi et al. 2006). The first black holes can potentially produce very intense ionizing radiation and due to their X-ray radiation are efficient at heating up the surrounding IGM.

In this paper, we use high resolution SPH simulations of massive, isolated ($3-4 \sigma$) halos to study the early growth and evolution of the first seed black holes and explore the impact of their evolution to reionization and X-ray heating. Semi-analytic models that consider plausible scenarios for the hierarchical assembly and growth of massive black holes from such seeds (Volonteri et al. 2003, 2005; Madau et al. 2004) have either assumed Eddington accretion or have argued that quasi-spherical, 'Bondi' accretion in halos with $T_{vir} > 10^4$ K, where efficient cooling via hydrogen atomic lines could occur, can sustain critical and short phases of supercritical accretion (Volonteri and Rees 2005). Multi-scale simulations that follow the hierarchical assembly history in Λ CDM of the most massive halos forming in a $\sim 3 \text{ Gpc}^3$ volume at $z \sim 6.5$ as well as the associated black hole growth have been able to show such rare massive halos are good candidates for the hosts of the first quasars (Li et al. 2006). Here, we follow these earlier papers in considering the hierarchical assembly of SMBHs and use the approach of direct SPH cosmological simulations to consider the physical conditions of the gas inflows that feed the central black hole in its early growth. Thanks to the faithful tracking of the gas dynamics these provide a self-consistent treatment of the coupling of large-scale gas inflow, black hole growth and associated feedback processes. In particular, we will base our treatment of accretion onto massive black hole and associated energy feedback on the method recently developed by Di Matteo et al. (2005); Springel et al. (2005b) in fully three-dimensional hydrodynamic simulations, where, for example, we were able to explicitly confirm that self-regulated quasar growth can reproduce the observed $M_{\text{BH}}-\sigma$ relation. We focus on understanding the black hole growth history at early time and as a function of halo mass. We do not impose a critical Eddington growth phase, but instead attempt to assess the detailed black hole accretion history (our work can thus be seen as complementary to Li et al. (2006)). Our aim is to test how reliable the assumption of Eddington growth is likely to be, in particular close to the time of reionization.

In §2 we review our simulation method and in particular the implementation of the black hole accretion and feedback model, as well as our recipe for seeding primordial minihalos with black holes. We then discuss the general properties and evolution of the black holes in simulations of halos of various masses (§3). We explore the implications of our results for BH growth scenarios as well as for the IGM reionization and heating in §4. In §5 we briefly summarize our main results. Throughout, a standard Λ CDM cosmological model is assumed, with $\Omega_\Lambda = 0.7$, $\Omega_m = 0.3$, baryon density $\Omega_b = 0.04$ and

Hubble constant $H_0 = 100h \text{ km/s/Mpc}$ ($h = 0.7$).

2. THE SIMULATION METHOD

2.1. SPH cosmological simulations

The simulations are performed with the parallel cosmological TreePM-Smooth Particle Hydrodynamics (SPH) code GADGET2 (Springel 2005). This code has been extensively tested in a wide range of applications from large scale structure formation to star formation. For the computation of the gravitational force, the code uses the Tree-PM method that combines a 'tree' algorithm for short range forces and a Fourier transform particle-mesh method for long range forces. GADGET2's implementation of SPH (e.g Monaghan 1992) uses a formulation which manifestly conserves energy and entropy while using fully adaptive SPH smoothing lengths (Springel and Hernquist 2002). Both the force computation and the time stepping of the code are fully adaptive. Radiative cooling and heating process are included (as in Katz et al. 1996), as is photoheating due to an imposed ionizing UV background. Detailed tests of the basic performance and accuracy of GADGET2 for gravitational and hydrodynamic problems are presented in Springel et al. (2005a).

The interstellar medium (ISM), star formation and supernovae feedback as well as black hole accretion and associated feedback are treated by means of sub-resolutions models. In particular, the multiphase model for star forming gas developed by Springel and Hernquist (2003a) has two principal ingredients: (1) a star formation prescription and (2) an effective equation of state (EOS). For the former we adopt a rate motivated by observations and given by the Schmidt-Kennicutt Law (Kennicutt 1989), where the star formation rate is proportional to the density of cold clouds divided by the local dynamical time and normalized to reproduce the star formation rates observed in isolated spiral galaxies (Kennicutt 1989, 1998). The effective EOS encapsulates the self-regulated nature of star formation due to supernovae feedback in a simple model for a multiphase ISM. In this model, a thermal instability is assumed to operate above a critical density threshold ρ_{th} , producing a two phase medium consisting of cold clouds embedded in a tenuous gas at pressure equilibrium. Stars form from the cold clouds, and short-lived stars supply an energy of 10^{51} ergs to the surrounding gas as supernovae. This energy heats the diffuse phase of the ISM and evaporates cold clouds, thereby establishing a self-regulation cycle for star formation. ρ_{th} is determined self-consistently in the model by requiring that the EOS is continuous at the onset of star formation. The cloud evaporation process and the cooling function of the gas then determine the temperatures and the mass fractions of the two 'hot and cold' phases of the ISM, such that the EOS of the model can be directly computed as a function of density. The approach we adopt here for star formation (and the parameters we use) has already been shown to lead to a numerically converged estimate for the cosmic star formation history of the universe that agrees well with low redshift observations (Springel and Hernquist 2003b).

A prescription for accretion and feedback from massive black holes is also included (Di Matteo et al. 2005; Springel et al. 2005b). Technically, we represent black holes by collisionless particles that grow in mass by accreting gas from their environments. A fraction of the

radiative energy released by the accreted material is assumed to couple thermally to nearby gas and influence its motion and thermodynamic state. Our underlying assumption is that the large-scale feeding of galactic nuclei with gas (which is resolved in our simulations) is ultimately the critical process that determines the growth of massive black holes. Here we briefly review the main features and ingredients of this model.

2.1.1. The seed black hole

There is no clear consensus for the mass of the first black holes. A number of scenarios exist which suggest that rather than starting out as stellar mass black holes, the first black holes are formed as intermediate mass black holes. ‘‘Seed’’ black holes can form as the end-point of the evolution of the first generation of stars (e.g Bromm et al. 1999; Abel et al. 2000; Nakamura and Umemura 2001; Yoshida et al. 2003; Gao et al. 2006) and in this case a BH of mass a few $100 - 10^4 M_\odot$ can result (e.g Madau and Rees 2001; Heger et al. 2003; Ricotti and Ostriker 2004). The most massive Pop III stars will form in rare high density peaks of the primordial density field (Gao et al. 2006). This will be the starting point for our study.

We introduce collisionless ‘sink’ particles in the simulations to model black holes at the centers of minihalos. In order to achieve this we keep track of the formation of minihalos by running a friends-of-friends (FOF) group finder. For reasons of performance, and because the identity of halos changes only slowly, the group finder is not run every timestep but at times equally spaced in log scalefactor, with $\Delta \log a = \log 1.25$. The group finder is run with a linking length of 0.16 and we select objects with a mass of $10^6 M_\odot$ and place a seed BH of $M_{\text{seed}} = 10^4 M_\odot$ in them if they do not already contain a BH. In practice most of the halos of this mass and their black holes are formed between $z = 15$ and $z = 30$.

Our choice of $M_{\text{seed}} = 10^4 M_\odot$ is on the high side for Pop III remnants. This mass corresponds approximately to the total available reservoir of star forming gas in these halos as found recently by Gao et al. (2006). In this work, the authors could not accurately predict how much of this gas would end up in the Pop III star and although they argued that the growth probably would stop before the stellar object reaches $10^3 M_\odot$ these results are subject to considerable uncertainty. Hence, here we have explored the most optimistic case (from the point of view of studying early SMBH formation from stellar seeds) in which all of the total gas reservoir of $10^4 M_\odot$ has gone into the formation of first star. In §4 we will however also discuss results for a more conservative value of $M_{\text{seed}} = 10^3 M_\odot$. Alternatively, these seeds can be viewed as the end results of direct gas collapse scenario or stellar gravitational collapse scenario (although these formation mechanisms are somewhat more speculative).

As we shall see the black holes do not undergo much evolution at early times, so our results are rather insensitive to the choice of the seeding procedure. In particular different choices for the linking length (the over-density) give similar results, although choosing it too low tends to select objects that have not yet completed collapse and that are extended and non-spherical. After the seeding of the BH by this procedure, further growth of the black hole sink particles proceeds by gas accretion, at a rate

that depends sensitively on the local gas conditions, or by mergers with other black hole particles.

2.1.2. Black hole accretion & feedback model

The accretion model is fully described and tested in Springel et al. (2005b); Di Matteo et al. (2005). We relate the (unresolved) accretion onto the black hole to the large scale (resolved) gas distribution using a Bondi-Hoyle-Lyttleton parameterization (Bondi 1952; Bondi and Hoyle 1944; Hoyle and Lyttleton 1939). In this description, the accretion rate onto the black hole is given by $\dot{M}_B = 4\pi [G^2 M_{\text{BH}}^2 \rho] / (c_s^2 + v_{\text{BH}}^2)^{3/2}$ where ρ and c_s are the density and sound speed of the ISM gas respectively, and v_{BH} is the velocity of the black hole relative to the gas. However, because of the strong dependence on sound speed of the Bondi accretion rate, the effective c_s resulting from our multiphase ISM model will give a poor estimate of the accretion rate. If we make the assumption that the time spent in the cold and hot phase of the ISM is proportional to their respective volume filling factors f_c and f_h , then formally

$$\begin{aligned} \dot{M}_B &= \frac{4\pi G^2 M_{\text{BH}}^2 f_c \rho_c}{(c_c^2 + v_{\text{BH}}^2)^{3/2}} + \frac{4\pi G^2 M_{\text{BH}}^2 f_h \rho_h}{(c_h^2 + v_{\text{BH}}^2)^{3/2}} \\ &= \frac{4\pi G^2 M_{\text{BH}}^2 x \rho}{(c_c^2 + v_{\text{BH}}^2)^{3/2}} + \frac{4\pi G^2 M_{\text{BH}}^2 (1-x) \rho}{(c_h^2 + v_{\text{BH}}^2)^{3/2}}. \end{aligned} \quad (1)$$

Here the subscripts c and h denote quantities in the cold and hot phase, x is the mass fraction in the cold phase, $x \equiv f_c \rho_c / \rho$. Normally the cold phase, and hence the first term in Equation 1, dominates the accretion rate. We use this expression to calculate the accretion rates from the local conditions at the BH positions. We also set a limit to the accretion rate by assuming the accretion rate cannot be higher than the Eddington rate, $\dot{M}_{\text{Edd}} \equiv (4\pi G M_{\text{BH}} m_p) / (\epsilon_r \sigma_T c)$ where m_p is the proton mass, σ_T is the Thomson cross-section, and ϵ_r is the radiative efficiency. The latter relates the radiated luminosity, L_r , to the accretion rate, \dot{M}_B as $\epsilon_r = L_r / (\dot{M}_B c^2)$, which simply gives the mass to energy conversion efficiency set by the amount of energy that can be extracted from the innermost stable orbit of an accretion disk around a black hole. We will adopt a fixed value of $\epsilon_r = 0.1$, which is the mean value found for a radiatively efficient (Shakura and Sunyaev 1973) accretion disk onto a Schwarzschild black hole.

As in Springel et al. (2005b), finally, we assume that a fraction ϵ_f of the radiated luminosity L_r couples to the surrounding gas in the form of feedback energy, viz. $\dot{E}_{\text{feed}} = \epsilon_f L_r = \epsilon_f \epsilon_r \dot{M}_B c^2$. For simplicity, we model this energy deposition as thermal energy deposited isotropically in the region around the black hole. Lack of spatial resolution precludes us from considering mechanical modes of releasing the energy, like jets and winds. However, it is likely that any form of black hole feedback will lead to a fraction of the energy being thermalized eventually, and that the final impact of the feedback depends primarily on the total amount of energy released and less on the form it is released in.

2.1.3. Black Hole Mergers

When two or more objects merge to form a single dark matter halo, dynamical friction on their central black

holes quickly brings them to the center of the halo where they are also expected to merge eventually - hierarchical black hole mergers contribute to the growth of the central black holes. However, whether black hole binaries coalesce efficiently is still a matter of debate. In a stellar environment, it has been argued that the binary hardens very slowly (Begelman et al. 1980; Milosavljević and Merritt 2003). In gaseous environments however binaries do coalesce more rapidly owing to strong dynamical friction within the gas (Makino and Funato 2004; Escala et al. 2004). In our galaxy-sized simulations (e.g. Di Matteo et al. 2005), and even more so in the cosmological top-hat models, it is not possible to treat in detail the problem of binary hardening. Because galaxies have typically large central concentration of gas we instead assume that two black hole particles merge if they come within the spatial resolution of the simulation (i.e. within the local SPH smoothing length) *and* their relative speed lies below the local sound speed. This could introduce a dependence of the derived merger rates on the resolution, however we will check that this is not the case (see §3.2.1).

In the final stage of the black hole mergers, the emission of gravitational waves carries linear momentum, which can cause the black hole to recoil (Madau et al. 2004; Volonteri and Rees 2006). Note that in our cosmological simulations we do not have the resolution nor the relativistic physics required to directly calculate the ejection of black holes by gravitational recoil. If the recoil is larger than the halo escape velocity the black hole will be ejected from its halo (Haiman 2004; Yoo and Miralda-Escudé 2004; Volonteri and Rees 2006). This effect is only important for similar mass mergers, moreover, the proper method to calculate the recoil velocity is still uncertain, leading to several order of magnitude variation according to different choices of parameters. We will discuss the possible implications of neglecting this effect in §4.

2.2. Initial Conditions

We set-up the initial conditions as isolated spherical overdensities that correspond to high- σ peaks in the Gaussian random field of cosmological density fluctuations (Katz 1991). In this configuration, the ‘top-hat’ (i.e. uniform density) cloud is given perturbations (using the Zeldovich approximation) with a given power spectrum $P(k) \propto k^{-2.5}$ appropriate for the scales we study. This is the same technique as that exploited recently by Bromm and Loeb (2003); Bromm and Larson (2004) in the treatment of the primordial star formation problem, except that here we are interested in larger halos ($T_{\text{vir}} > 10^4$ K) which cool efficiently via atomic hydrogen lines and for which H_2 cooling is not important.

Specifically, the following procedure is employed to set up the particle positions and velocities: first, a regular grid of dark matter (DM) particles is setup. The DM particles are assigned perturbations using the Zeldovich approximation, which also sets the peculiar velocities. The amplitude is normalized as in Bromm et al. (2002) by fixing the initial variance σ_i of the fluctuation spectrum at the starting redshift z_i ,

$$\sigma_i^2 = A \sum k^n, \quad (2)$$

such that

$$\sigma(z_{\text{vir}}) = \frac{1 + z_i}{1 + z_{\text{vir}}} \sigma_i = 1, \quad (3)$$

where z_{vir} is the target redshift of collapse (i.e. virialization). Particles from a spherical region of size $R = (3M/4\pi\rho)^{1/3}$ are then selected and given a Hubble expansion (modified to affect a collapse at the target redshift). A pre-determined amount of angular momentum is imparted by assigning rigid rotation to the particles with a spin parameter $\lambda = L|E|^{1/2}/GM^{5/2}$, where L is the angular momentum, $|E|$ the total energy and M the total mass. This is necessary because we cannot follow self-consistently the angular momentum evolution of the collapsing object. Gas particles are setup in the same way, except that they are not subject to the random perturbations, as on these scales pressure forces will have erased any initial density fluctuations.

2.3. The simulation parameters

Using the above procedure we can investigate different collapse scenarios by choosing the total mass M , the redshift of collapse z_{vir} and λ . In Table 1, we summarize the simulation parameters of the systems we examine. They comprise halos of $M = 10^8, 10^9, 10^{10}$ and $10^{11} M_\odot$. For z_{vir} we will take the collapse redshift of a $3\text{-}\sigma$ peak (for $\sigma_8 = 0.9$, for a $\sigma_8 = 0.75$ these would be $\approx 3.3\text{-}\sigma$) of the corresponding mass, i.e. $z_{\text{vir}} = 16, 12, 10$ and 7.5 respectively for these halos. Note, however, that in dense regions, likely the precursors of the halos that harbor high redshift quasars, high density peaks are over-represented, as found e.g. in recent numerical investigations by Gao et al. (2005) (where for example the precursor of simulated halos reach $10^8 M_\odot$ at redshift $z = 24$, $10^9 M_\odot$ at $z = 20$, $10^{10} M_\odot$ at $z = 16$ and $10^{11} M_\odot$ at $z = 10$). Thus we will also investigate a scenario with higher z_{vir} for the above mentioned range in halo masses, corresponding to $\sim 4\text{-}\sigma$ peaks. We take $\lambda = 0.03$ as the standard spin parameter for our runs. This value is consistent with the average spin parameter found in cosmological simulations (e.g. Jang-Condell and Hernquist 2001). We have also run our simulations using $\lambda = 0$ or $\lambda = 0.05$, and found no significant differences in our results (see also Bromm and Loeb 2003). For the runs we take $N = 10^5 - 10^7$ particles and a corresponding spatial resolution of a few tens to a hundred parsec.

An important parameter for our study is the value of the BH feedback factor. We will consider two extreme values: $\epsilon_f = 0$ corresponding to the case without feedback and $\epsilon_f = 0.05$, the value that has been used to reproduce the observed normalization of the local $M_{\text{BH}}\text{-}\sigma$ in galaxy merger simulations (Di Matteo et al. 2005). All simulations are run to a final redshift of about $z = 6$. After the collapse redshift there is no further infall of material or merging in these models, so the top-hat is not a reliable tool to investigate evolution of structure after this time.

3. RESULTS

3.1. The evolution of the central host and the seed black hole population

In Figure 1 we show a short sequence of projections of the baryon distribution (color coded by temperature) of the A3 run, representative of the simulations presented

here. The sequence starts at redshift $z = 20$ and ends at the redshift of collapse $z_{\text{vir}} \sim 10$. Each panel is 200 kpc (comoving) on the side. As expected, the over-dense region initially expands with the Hubble flow at a reduced rate and subsequently turns around (at $z \sim 16 - 17$) and eventually collapses. The evolution of the central object, as well as the formation of substructure follows the general scenario of structure formation in a Λ CDM cosmology. Briefly after turn around, the dark matter component has developed significant substructure and baryons start falling into the deepest potentials, black holes are formed and star formation eventually ensues (the only black holes shown in Figure 1 are the most massive and those twice the initial seed mass). Close to the redshift of virialization, $z_{\text{vir}} \sim 10$ the halo undergoes violent relaxation, with the gas settling in the central regions.

Figure 2 shows a more detailed view (10 kpc proper) of the gas distribution and a simulated rest-frame UBV I image composite just before final collapse at $z \sim 10$. At this point, what looks like a heavily obscured star bursting system fed by remnant bridges and filaments of HI gas, is about to merge with two other smaller systems. Blue colors show the intense star formation going on (the star formation rate is about $1.5 M_{\odot}/\text{yr}$), indicating the general youth of the system. The total star mass is about $5 \times 10^7 M_{\odot}$ (see Fig. 3). The remaining massive black holes (that have not yet merged) and their associate feedback energy give rise to the faint low density bubbles in the gas distribution (e.g.; in the lower right object of the bottom panel of Fig. 2). The total mass of black holes at $z = 10$ is $6.3 \times 10^6 M_{\odot}$, with the heaviest, at the center of the collapsing halo, accounting for 10% of that. Further evolution of this system will form an elliptical dwarf galaxy after the gas reservoir is depleted (at $z = 6$ the star formation rate has markedly leveled off, see Figure 3).

Within our model the formation of seed BH mirrors the evolution of substructure in the halo. The growth of the cumulative BH mass function and the evolution in the number of BHs are shown in Figure 4 and Figure 5 respectively. At $z = 20$ the number of BH is still low, commensurate with the lack of structure at masses scales of $10^6 M_{\odot}$ in the parent halo. However as substructure forms in the simulation, the formation rate of BHs increases, peaking at $z = 16$ (as expected this is close to the turnaround redshift for this halo). Most BHs have just formed and therefore the mass function peaks at around the seed mass value. At a redshift $z = 12$ (lower left panel of Figure 1) the growth rate is offset by the merger rate and the number of BH reaches a maximum. The BH mass function has grown significantly at most mass scales.

Further evolution of the collapsing halo decreases the number of BHs because of the merging of sub-halos (and the corresponding mergers of central BHs). This is reflected by the more significant growth in the high mass tail of the mass function. Finally, at the redshift of collapse the merger rate of BH peaks, resulting in a rapidly declining number of BH in the lower mass end and a fast growth of the central massive object. Also shown in Figure 5 are the resulting BH counts for the C3 run. In this case the collapse occurs at higher redshift, and the evolution of the number of BHs happens at correspondingly

earlier times. It is otherwise similar to the A3 case, with the peak formation rate in this case occurring at $z = 24$.

As shown in Figure 3, up to about the turn-around redshift of the halo the total black hole mass density is higher than the star density, but as significant cooling of the gas ensues after this time, star formation becomes significant and the resulting star mass density quickly exceeds the black hole mass after $z \sim 12$, the growth of which has virtually saturated by $z \sim 10$. This is also reproduced in the C3 run, where the cross over point for the star density to exceed the black hole mass is at commensurately higher redshift ($z \sim 22$).

We can obtain an estimate of the global black mass function by taking our simulations to be representative for halos of that mass and multiplying the corresponding number of BHs in each black hole mass bin by the expected number density of halos of that mass and summing over the mass range of our simulations,

$$n(M_{\text{BH}} > M) = \sum_i n_i N_i(M_{\text{BH}} > M) \quad (4)$$

with number densities n_i estimated using the Press-Schechter formalism. This is shown in Figure 6. The basic picture that emerges from this is that low mass BH population builds up early, and as heavier halos collapse the range gradually expands to higher masses, in agreement with Figure 4. The low end of the mass function does not fall (or at least not as much as in Fig. 4), because the high mass halos contribute comparatively less to the low mass population of BH.

In the next section we will discuss our results on the growth history of the massive black hole in the center of the collapsing halo as a function of halo mass.

3.2. BH growth and accretion history

Figure 7 shows the evolution of the black hole mass (top panels) and accretion rate (bottom panels) for the most massive black hole formed at the center of the collapsed halos. The major BH is traced through its most massive progenitor back to the first seed, which forms at a redshift of around $z \sim 20$ for the majority of our simulations. The accretion rate and the black hole mass are shown for runs for which we have included BH feedback and for runs with with no BH feedback (A1-A4 and B1-B4 in Table 1). For the $10^{10} M_{\odot}$ halo, the results for an intermediate feedback strength ($\epsilon_f = 0.01$) are also shown.

If we compare the runs of different mass halos with and without feedback the impact of BH feedback becomes clear: even with modest levels of feedback (5% of the radiative energy in most cases, also shown is the case of 1% for the $10^{10} M_{\odot}$ halo) the growth of the black hole is severely limited compared to the case with zero feedback. In the models with no feedback the accretion rate starts off at values of the order or $10^{-6} M_{\odot} \text{yr}^{-1}$, much the same as the models with feedback. However, while in the feedback runs the average accretion rate stays well below the critical values (by at least a factor of 100), in the zero feedback case the typical accretion rates reach the Eddington values leading to a fast growth of the black hole mass. Even in this case, however, the critical accretion phase is reached only close and subsequent to the time of final collapse of the halos (i.e. only at $z < 10$); accretion is sub-Eddington before that. As shown by the

discrete jumps in the black hole mass evolution in Figure 7, the growth of the central black hole is dominated by black hole mergers up to the time it reaches the critical accretion phase. In models with BH feedback, gas accretion also becomes increasingly more important as the halo mass increases (and hence the central gas densities increase). As the accretion rate increases and the BH becomes heavy enough, the feedback energy associated with accretion, is able to heat the gas sufficiently to “shut off” any further growth. This occurs rather abruptly. The greater the mass of the halo, the longer the simulation with feedback follows (approximately) the growth curve of the simulation without feedback. Hence the difference is smallest for the $10^{11} M_{\odot}$ run. Figure 7 shows that the difference in evolution of black hole accretion rate and hence final black hole masses in models with and without BH feedback increases for smaller halo mass runs. For the $10^{11} M_{\odot}$ run the accretion rates are similar up until the time close to the collapse (at $z \sim 7.5$). At this point, the growth barely reaches the critical Eddington value, while lower mass runs with feedback do not reach Eddington growth at all. So this mass may be considered the minimum mass for any efficient black hole growth relevant to quasar activity. Still, only a fraction of the final black hole mass ($\sim 10\%$) results from mass accretion in this case. At lower mass scales the growth is more inefficient still, occurring mostly due to BH-mergers (for the $10^8 M_{\odot}$ case less than 1% is due to accretion). This means that the masses derived are sensitively dependent on the assumed seed masses.

Note that for the runs without feedback the BH starts to grow at the Eddington rate eventually, not from the onset of BH formation, but only after a significant number of mergers have occurred. When growth at the Eddington rate does start, an exponential runaway growth phase occurs. In this case $\lesssim 5\%$ of the final mass of the BH consists of the original seed masses. At the end of the simulations, we see that the final BH masses are proportionally larger for larger halo masses, except for the $10^{11} M_{\odot}$ simulation, because in this case the time after the z_{vir} is comparatively much shorter than for the other simulations, leaving too little time for all the BH mergers and much of the significant accretion phase to occur (as we have stopped all simulations at $z_{\text{end}} = 6$).

In order to better appreciate the cause of the differences in the BH accretion history for the cases with and without feedback, we show in Figure 8 the evolution of the physical quantities that determine the growth of the black hole in our model. The gas density around the BH in the model with feedback has lower density, as well as higher sound speed than the in run without feedback. This is expected due to the local heating associated with the BH feedback which eventually energizes the gas sufficiently to drive a slow wind (Springel et al. 2005a). Figure 8 also shows that the relative BH-gas velocities are higher in the feedback case: if no feedback is included the gas settles in a quiet equilibrium which is most efficient at feeding the central BH (note that the decrease in density and sound speed at the end of the B1 run is a result of gas depletion due to runaway BH growth). The effect of BH feedback on its surroundings is also visible in the much stronger variations in density and sound speed, indicating that the ISM around it is being stirred, and definitely not in equilibrium. This is consistent with the

gas density projection in Figure 2 which shows the faint bubbles blown in the ISM as a result of the BH feedback.

3.2.1. Resolution tests

In order to assess possible resolution effects on our results, we have carried out resolution tests. Figure 9 shows the black hole mass for the $10^{10} M_{\odot}$ halo with three different particle numbers ($N = 10^5, 10^6, 5 \times 10^6$) spanning a factor of 50. The results show consistent black hole growth. In particular, the final BH mass is rather insensitive to the resolution used. The lowest resolution run ends up with 40% lower BH mass due to the fact that there is some loss in resolution of the substructure that would form extra BH at high resolution, but the two higher resolution runs show convergence for the final BH mass within 10%. Even though at high redshifts there is some disparity between the runs at different particle numbers, there is no systematic trend with particle number. Some differences are expected due to the stochastic nature of the BH merger growth in our simulations, which tend to magnify small differences in BH trajectories at different resolution. We consider our results to be reliable at the medium resolution, although for highest mass halos we use the higher particle count.

4. DISCUSSION

Our results caution against the commonly made assumption for the early black hole growth, namely that they accrete at the Eddington rate (e.g. Haiman 2004; Yoo and Miralda-Escudé 2004; Madau et al. 2004; Volonteri and Rees 2006). We have shown that this is likely an overestimate of the growth rate, and may consequently lead to overly optimistic mass estimates for the central black holes masses of the first quasars. In our simulations, seed black holes typically accrete well below the critical Eddington rates. For halos $M \leq 10^{10} M_{\odot}$ BHs never reach an Eddington growth phase, or if they do, it is only at the time close to the collapse redshift and under the rather extreme assumption that any kind of black hole feedback is switched off. The growth reaches the Eddington rate at late times only for halos of $M \geq 10^{11} M_{\odot}$. The final black hole masses at the time of collapse are proportional to the total halo mass with

$$M_{BH} = 5 \times 10^6 M_{\odot} (M_{\text{halo}}/10^{11} M_{\odot})^{0.78} \quad (5)$$

(Fig. 10). For the highest mass halo this implies a black hole mass of $M_{BH} \sim 10^7 M_{\odot}$, a couple of orders of magnitude below the values deduced for the $z = 6$ Sloan quasars. Our results therefore imply that the first black holes, remnant from the first generation of stars, are unlikely to grow into the first quasars unless the Sloan quasars are hosted in halos rarer than 3-4 σ peaks. If we compare the number density in halos inferred from the space density of quasars at $z = 6$ (Fan et al. 2004) this requires that their host masses be larger than those studied here, and of the order of $10^{13} M_{\odot}$ typical of an extremely rare 5.5- σ (or higher for WMAP3) peak (note however that this assumption corresponds to a duty cycle of order unity for the Sloan quasar). An extrapolation of Figure 10 (using Eq. 5) gives a BH mass of $\sim 10^8 M_{\odot}$ for a $10^{13} M_{\odot}$ halo (independent of z_{vir}), which falls short by a factor of $\gtrsim 10$ with respect to the inferred SDSS quasar masses. If taken at face value, Equation 5 implies a minimum halo mass of $10^{14} M_{\odot}$, which represents a $> 8\text{-}\sigma$

peak at $z = 6$. Such peaks are much too rare. An earlier collapse redshift for the $10^{13} M_{\odot}$ halo may allow the BH mass to grow to the SDSS values (assuming the Eddington growth is sustained after the virialization of the parent halo). The collapse would then be required to occur at least $\Delta z \approx 0.5$ earlier. This shifts the $5.5\text{-}\sigma$ peak to even higher σ and again makes the parent halo a factor 20 – 50 too rare.

These rather stringent conclusions on the inefficiency of seed growth are reached despite the fact that we have made rather optimistic assumptions regarding BH growth. Namely, we have assumed that all halos of a certain mass will host a seed BH (thus without taking into account possible feedback effects from the formation events of these BHs on nearby halos). Furthermore, the seed BHs we assume to be formed are massive, certainly in the upper range of masses considered for BH seeds from remnant Pop III stars. However, the rather slow black hole growth implied by our results makes the problem a rather strong function of the initial choice of seed mass (as most of the growth occurs at the Bondi rate or via mergers instead of an exponential Eddington phase). Smaller seed masses than the value chosen here would imply even slower growth. This is illustrated in Figure 7, where, for the $10^{11} M_{\odot}$ run we have also plotted a rerun of the A4 simulation, but with a seed mass of $M_{\text{seed}} = 10^3 M_{\odot}$. In this case the final mass is more than a factor 10 smaller, as expected. Note however that the BH in this case also reaches Eddington growth. This again shows that a halo mass of $\sim 10^{11} M_{\odot}$ is sufficient for Eddington growth. Larger seed masses would allow faster growth. However, larger seeds (e.g. $\sim 10^5 M_{\odot}$) than the ones we have chosen would merely emphasize the need of a jump-start scenario for the formation of the $z = 6$ Sloan quasars. Using detailed simulations, Li et al. (2006) have shown that halos of $10^{13} M_{\odot}$ could be the hosts of the first quasar. However, in their work it was assumed that BH would undergo growth at the Eddington rate, preceding the time of major mergers at $z \sim 7 - 12$. This isolated critical growth phase implies masses $\sim 10^5 M_{\odot}$ upon entering major mergers. Furthermore they used fully assembled galaxies models as their initial conditions, thus not following the assembly of galaxies and their BH self-consistently.

One feature of our modeling that stands out as being inconducive to BH growth is the inclusion of BH feedback. Even though the exact mechanism by which the AGN acts on its surrounding ISM is poorly understood, it is likely that the end-effect of AGN feedback is that a fraction of the accreted rest mass energy is thermalized in the surrounding medium, which is what we consider. The amount of feedback energy we use is a rather moderate 0.5% of the rest mass of the infalling material. We have also shown that simulations with $5\times$ lower feedback strengths (see Fig. 7) yield qualitatively similar results. Any amount of black hole feedback is therefore expected to affect the black hole growth rather dramatically regardless of the details of the feedback processes.

The multiphase model we use for the star forming ISM takes into account that we have limited resolution to follow the densest phases of the ISM. Nevertheless, this introduces some dependence on the choice of model parameters. For example the critical density for star formation might be a function of the chemical composition. Higher

critical densities would give a higher mean density for the ISM, leading more rapid growth. It is unlikely, however, that the star formation model in these early objects is radically different, because star formation is locally seen to proceed in much the same way for a wide variety of environments, amongst which very low metallicity ones.

For our choice of parameters almost all BH mass ends up in one central BH (Fig. 5). This is, to some extent, the result of our simplified criterion that leads to BH mergers. Clearly, different assumptions are likely to decrease the merger rate, even though, in general, the view is that the friction processes that bring two BHs into close vicinity of each other will operate efficiently (e.g. Begelman et al. 1980; Chatterjee et al. 2003). Here we do not take into account the effects of momentum carried away by gravitational waves. This so called “gravitational recoil” (GR) can expel BH from their parent halos instead of merging them. This effect was examined in semi-analytical models by Haiman (2004), Yoo and Miralda-Escudé (2004) and more recently by Volonteri and Rees (2006). Haiman found that GR will inhibit BH growth unless recoil velocities are smaller than $\sim 65\text{km/s}$. Yoo and Miralda-Escudé (2004), on the other hand, managed to grow BH to $10^9 M_{\odot}$ by $z \approx 10$ for slightly different assumptions regarding the GR strength and the escape velocities from halos, with about equal contributions from BH mergers and gas accretion processes. In either case, the authors did however make the assumption that the fueling of the BH is sufficiently effective to support BH growth at the Eddington rate. Interestingly, Yoo and Miralda-Escudé (2004) have examined the effects of restricting the gas accretion to halos of a minimum velocity dispersion. They found that for the upper ranges of the threshold dispersion they considered the BH growth was severely impeded, which is consistent with our findings. Such a threshold would be somewhat ad-hoc in their model, whereas we find that indeed this restricted mode of accretion is more realistic due to the feedback effects.

Volonteri and Rees (2006) explore the conditions for the growth of seeds up to the SDSS quasars again assuming that this occurs at the Eddington rate. In particular, they consider the impact of dynamical effects of gravitational recoil. Their main conclusion is that the occurrence of SMBH at early times is very selective. They argue that SDSS quasars could be hosted in halos of $M \sim 10^{11} M_{\odot}$, provided that the radiative efficiency is not too high, as in this case they are likely not to suffer significantly from the negative contribution due to dynamical effects. Alternatively for growth in higher halo masses ($10^{13} M_{\odot}$ or so) the kick velocities need to be considered at the low end. Our results however highlight the difficulty of sustaining Eddington growth in the first place in halos of $M \sim 10^{11} M_{\odot}$, arguing for even more selective conditions that allow for rapid growth.

Faced with the difficulty of growing seed BHs to the Sloan quasars, some authors propose that short phases of super-Eddington growth can jump start the growth of BHs. In particular, Volonteri and Rees (2005) proposed a scenario in which BH grow in thick and dense ($n = 10^4 \text{cm}^{-3}$, $T = 8000 \text{K}$) gas disks formed at very high redshift, at $z \sim 20$ before the universe is enriched and metal cooling can affect collapse and fragmentation. These authors argue that the BH should accrete gas at

rates comparable to the Bondi estimate, which for these conditions far exceeds the Eddington rate. In our model, the implicit assumption for the ISM is that some enrichment has taken place as a result of the PopIII star formation, significantly enough that star formation is proceeding and feedback from SN and stellar winds pressurizes the ISM, inhibiting the formation of large and dense central disks as those inferred by Volonteri and Rees (2005). We cannot therefore directly probe the scenario of super-critical accretion proposed but ultimately the conclusion from that work also requires extremely rare host for the Sloan quasars.

In our simulations we have not treated the detailed physics of HII regions of the first stars in the ISM surrounding the first black holes at $z \sim 20$ (rather we have optimistically assumed efficient HI cooling). Johnson and Bromm (2007) have recently shown that the seed black hole growth may experience an additional early bottleneck due to significant delay between black hole formation and the onset of efficient accretion in the primordial HII gas. This work strengthens our results, and in general the argument that it may be hard to grow the first quasars from the remnants PopIII black holes.

4.1. Reionization and X-ray heating

Several authors have recently investigated the potential impact of a primordial generation of BHs on the reionization process and the thermal evolution of the IGM. More specifically, high- z BHs could produce a substantial amount of ionizing photons due to their potentially higher luminosity compared to stellar type sources (per unit mass accreted) and likely higher escape fraction (e.g. Madau et al. 1999; Valageas and Silk 1999; Miralda-Escudé et al. 2000; Wyithe and Loeb 2003; Madau et al. 2004). In addition, their harder spectra would also induce reionization of HeII, otherwise unattainable with stellar type sources (with the exception of very massive PopIII stars). Finally, X-ray photons could produce a fairly homogeneous reionization (due to their large mean free path), albeit not complete (e.g. Oh 2001; Venkatesan et al. 2001; Madau et al. 2004; Ricotti and Ostriker 2004), and substantially heat the IGM. Most of these calculations however have also been carried out under the assumption that the first black holes are growing at the critical Eddington rate at early time. Here, we briefly investigate the implication of the black hole accretion history we obtain from our simulations for ionization and X-ray heating of the IGM. We will limit ourselves to some simple estimates, deferring a more detailed investigation to a future paper.

The production rates of ionizing photons $h\nu > 13.6$ eV is plotted in Figure 11 for the various halo masses we have simulated. The rate of ionizing photons from stars ϕ_\star is calculated as $\phi_\star = \psi_\star \dot{M}_\star$, where \dot{M}_\star is the star formation rate and $\psi_\star = 3 \times 10^{60}$ photons/ M_\odot is the yield, typical of a stellar population with salpeter IMF and a metallicity of about 1% Solar. In the case of metal-free, massive stars, ψ_\star can be more than an order of magnitude higher (as discussed above our assumption is that in general some enrichment has taken place). Thus, the stellar production rate of ionizing photons should be regarded as a lower limit. We calculate the BH photon production rate assuming that all radiation comes out as ionizing photons with a mean energy of $\langle h\nu \rangle = 80$ eV (such a hard

spectrum is justified for smaller mass BH, e.g. Madau et al. (2004)). This gives a production rate for BH of $\phi_{\text{BH}} = \psi_{\text{BH}} \dot{M}_{\text{BH}}$, with $\psi_{\text{BH}} = 1.5 \times 10^{63}$ photons/ M_\odot .

From Figure 11 it is clear that the stellar contribution to the overall budget of ionizing photons is dominant, with the exception of $z \sim 17 - 20$ in the larger objects. Note some episodes of high luminosity occur at high redshift for the BH, when accretion rates peak momentarily before being quenched by BH feedback (such episodes of increased accretion are also visible in Fig. 7), but they are too short to affect the ionization much. It should be noted, however, that the escape fraction (i.e. the fraction of emitted ionizing photons that are able to escape in the IGM) for stellar photons is likely to be smaller than that for photons produced by BH, which might thus be relevant during certain epochs of structure evolution.

We estimate the total production of ionizing photons n_{ph} , similar to our estimate of the total mass function, by multiplying the cumulative production of ionizing radiation of each halo by their expected number density and summing over the mass range of our simulations,

$$n_{ph}(t) = \sum_i n_i \int_0^t \phi_i dt \quad (6)$$

with number densities n_i estimated using the Press-Schechter formalism. Figure 12 shows the contribution of stars and BH to the cumulative number density of ionizing photons (normalized on the global hydrogen number density). The contribution from the stars under the above assumption for the ionizing photon flux and with an escape fraction of 100% for both components is an order of magnitude larger at all redshifts. If the gas is distributed uniformly and does not recombine, we have a reionization redshift of $z \sim 12$. This conclusion is not affected by the contribution to ionization from the BHs.

One of the most interesting effects of the harder radiation by BHs is IGM heating due to X-rays. As X-rays are much more likely to be absorbed by HeI rather than HI (due to the higher cross section), direct photoionization of HI by X-rays is negligible. Nevertheless, the electron ejected by HeI photoionization is more likely to ionize HI than HeI because the former is much more abundant. The partitioning of a photoelectron energy between heating the gas and secondary ionization is a function of the gas ionization fraction. For values above 10% most of the energy goes into heating. For this reason, although HI ionization by X-rays is not likely to exceed 30%, heating of the IGM up to temperatures of $\sim \text{few} \times 10^3$ K can be rapidly obtained (Shull and van Steenberg 1985). This has interesting implications on the observability of the reionization process at high redshift. In fact, a powerful probe of the neutral IGM is 21 cm line emission associated with the spin-flip transition of the ground state of HI. In order to observe such a line in emission, the gas temperature needs to be higher than the CMB temperature. X-rays from microquasars provide the most viable and uniformly distributed heating source available (e.g. Chen and Miralda-Escudé 2004; Kuhlen et al. 2006). The temperature reached by the IGM subject to a soft X-ray background due to accretion onto BH can be estimated as (Madau et al. 2004)

$$T \approx 75 \text{ K} \left(\frac{f_{\text{heat}}}{0.13} \right) \left(\frac{\rho_{\text{acc}}}{10 M_\odot / \text{Mpc}^3} \right) \quad (7)$$

with comoving accreted mass density ρ_{acc} ($\rho_{\text{acc}} = 10 M_{\odot}/\text{Mpc}^3$ at $z \sim 18$ for our results) and the fraction f_{heat} of the X-ray energy going into heating the gas, depending on the ionization fraction (values for f_{heat} range from $f_{\text{heat}} \approx 0.13$ to $f_{\text{heat}} \approx 0.6$, Shull and van Steenberg (1985)). As we have discussed, ρ_{acc} is typically smaller than ρ_{BH} as most the black hole mass is built up by BH-mergers.

Summing the total accretion rate over the $3\text{-}\sigma$ halos with $M_{\text{halo}} = 10^{8-11} M_{\odot}$ as for the ionizing photon production estimate, we see (Fig. 13) that heating by BH accretion becomes important in our model at $z \lesssim 15-18$ (depending on f_{heat}), somewhat later than the redshifts $z \approx 22$ found by Madau et al. (2004), whose ρ_{acc} already approached a few hundreds M_{\odot}/Mpc^3 at that redshift. The temperatures we find for $z \lesssim 15-18$ is in the range $300-1000$, which are somewhat lower than those found by Kuhlen and Madau (2005). X-rays from SN remnants, shocks associated with structure formation and Ly- α photons may also aid the IGM heating process.

5. CONCLUSIONS

In this paper we have assessed the early growth and evolution of BH seeds assumed to form with $M_{\text{seed}} \sim 10^4 M_{\odot}$ (an optimistic value) as end product of the very first generation of PopIII stars or by direct collapse of gas at $z \sim 20-30$. We have used direct SPH simulations with a simple prescription for BH gas accretion and associated feedback to explore the early accretion history of seed black holes in halos of mass $10^8-10^{11} M_{\odot}$, representative of the typical 3-4 σ halos collapsing at $20 < z < 6$. We have focused on constraining the gas accretion history onto the seed black holes to compare with the widely adopted assumption that at these times seed BHs grow at the Eddington rate. The latter is required if such seed black holes are to explain the masses associated with $z \sim 6$ quasars (without postulating a phase of supercritical accretion as invoked by Volonteri and Rees (e.g. 2005)). In addition, Eddington accretion is generally assumed when estimating the impact of mini-quasar

to reionization and their role heating the IGM. We found that:

- seed BHs inhabiting halos of $< 10^{11} M_{\odot}$ do not reach an Eddington rate accretion phase. The growth reaches the Eddington rate at late times only for halos of $M \geq 10^{11} M_{\odot}$. Due the limited time spend in an Eddington growth phase it is difficult to explain the occurrence of the $z \sim 6$ SDSS quasars.
- feedback from the BHs is very effective impeding BH growth. Unless feedback processes operate at these high redshifts differently such that black hole feedback return $\ll 0.005$ of the rest-mass energy of the infalling material to the ISM, its effects leads to a significant delay for the onset of the Eddington growth phase.
- the main growth of BHs in these objects occurs mainly through BH mergers. The final masses of the central most massive black hole scales as $M_{\text{BH}} \sim 5 \times 10^6 (M_{\text{halo}}/10^{11} M_{\odot})^{0.78}$. Because critical accretion rates are hard to reach in these halos, the final BH masses depend on the initial seed mass.
- miniquasars are not likely to contribute significantly to reionization.
- X-ray heating resulting from underfed miniquasars is however likely sufficient to cause significant IGM heating by $z \sim 15$.

The computations reported here were performed at the Astrophysics Theory Cluster at Carnegie Mellon University and at the Pittsburgh Supercomputer Center (PSC), a leading edge site in the NSF Shared Cyberinfrastructure. TDM acknowledges partial support for this project from NSF grant AST-0607819.

REFERENCES

- Abel, T., Bryan, G. L., & Norman, M. L., 2000, *ApJ* **540**, 39
 Begelman, M. C., Blandford, R. D., & Rees, M. J., 1980, *Nature* **287**, 307
 Begelman, M. C., Volonteri, M., & Rees, M. J., 2006, *MNRAS* **370**, 289
 Bondi, H., 1952, *MNRAS* **112**, 195
 Bondi, H. & Hoyle, F., 1944, *MNRAS* **104**, 273
 Bromm, V., Coppi, P. S., & Larson, R. B., 1999, *ApJ* **527**, L5
 Bromm, V., Coppi, P. S., & Larson, R. B., 2002, *ApJ* **564**, 23
 Bromm, V. & Larson, R. B., 2004, *ARA&A* **42**, 79
 Bromm, V. & Loeb, A., 2003, *ApJ* **596**, 34
 Chatterjee, P., Hernquist, L., & Loeb, A., 2003, *ApJ* **592**, 32
 Chen, X. & Miralda-Escudé, J., 2004, *ApJ* **602**, 1
 Di Matteo, T., Springel, V., & Hernquist, L., 2005, *Nature* **433**, 604
 Eisenstein, D. J. & Loeb, A., 1995, *ApJ* **443**, 11
 Escala, A., Larson, R. B., Coppi, P. S., & Mardones, D., 2004, *ApJ* **607**, 765
 Ferrarese, L. & Merritt, D., 2000, *ApJ* **539**, L9
 Gao, L., White, S. D. M., Jenkins, A., Frenk, C. S., & Springel, V., 2005, *MNRAS* **363**, 379
 Gao, L., Yoshida, N., Abel, T., Frenk, C. S., Jenkins, A., & Springel, V., 2006, *ArXiv Astrophysics e-prints*
 Gebhardt, K., Bender, R., Bower, G., Dressler, A., Faber, S. M., Filippenko, A. V., Green, R., Grillmair, C., Ho, L. C., Kormendy, J., Lauer, T. R., Magorrian, J., Pinkney, J., Richstone, D., & Tremaine, S., 2000, *ApJ* **539**, L13
 Greenstein, J. L. & Matthews, T. A., 1963, *Nature* **197**, 1041
 Haehnelt, M. G. & Rees, M. J., 1993, *MNRAS* **263**, 168
 Haiman, Z., 2004, *ApJ* **613**, 36
 Heger, A., Fryer, C. L., Woosley, S. E., Langer, N., & Hartmann, D. H., 2003, *ApJ* **591**, 288
 Hoyle, F. & Lyttleton, R. A., 1939, in *Proceedings of the Cambridge Philosophical Society*, p. 405
 Jang-Condell, H. & Hernquist, L., 2001, *ApJ* **548**, 68
 Johnson, J. L. & Bromm, V., 2007, *MNRAS* **374**, 1557
 Katz, N., 1991, *ApJ* **368**, 325
 Katz, N., Weinberg, D. H., & Hernquist, L., 1996, *ApJS* **105**, 19
 Kennicutt, R. C., 1989, *ApJ* **344**, 685
 Kennicutt, R. C., 1998, *ApJ* **498**, 541
 Koushiappas, S. M., Bullock, J. S., & Dekel, A., 2004, *MNRAS* **354**, 292
 Kuhlen, M. & Madau, P., 2005, *MNRAS* **363**, 1069
 Kuhlen, M., Madau, P., & Montgomery, R., 2006, *ApJ* **637**, L1
 Li, Y., Hernquist, L., Robertson, B., Cox, T. J., Hopkins, P. F., Springel, V., Gao, L., Di Matteo, T., Zentner, A. R., Jenkins, A., & Yoshida, N., 2006, *astro-ph/0608190*
 Loeb, A. & Rasio, F. A., 1994, *ApJ* **432**, 52
 Madau, P., Haardt, F., & Rees, M. J., 1999, *ApJ* **514**, 648

- Madau, P. & Rees, M. J., 2001, *ApJ* **551**, L27
- Madau, P., Rees, M. J., Volonteri, M., Haardt, F., & Oh, S. P., 2004, *ApJ* **604**, 484
- Magorrian, J., Tremaine, S., Richstone, D., Bender, R., Bower, G., Dressler, A., Faber, S. M., Gebhardt, K., Green, R., Grillmair, C., Kormendy, J., & Lauer, T., 1998, *AJ* **115**, 2285
- Makino, J. & Funato, Y., 2004, *ApJ* **602**, 93
- Milosavljević, M. & Merritt, D., 2003, *ApJ* **596**, 860
- Miralda-Escudé, J., Haehnelt, M., & Rees, M. J., 2000, *ApJ* **530**, 1
- Monaghan, J. J., 1992, *ARA&A* **30**, 543
- Nakamura, F. & Umemura, M., 2001, *ApJ* **548**, 19
- Oh, S. P., 2001, *ApJ* **553**, 499
- Ricotti, M. & Ostriker, J. P., 2004, *MNRAS* **352**, 547
- Schmidt, M., 1963, *Nature* **197**, 1040
- Shakura, N. I. & Sunyaev, R. A., 1973, *A&A* **24**, 337
- Shull, J. M. & van Steenberg, M. E., 1985, *ApJ* **298**, 268
- Springel, V., 2005, *MNRAS* **364**, 1105
- Springel, V., Di Matteo, T., & Hernquist, L., 2005a, *ApJ* **620**, L79
- Springel, V., Di Matteo, T., & Hernquist, L., 2005b, *MNRAS* **361**, 776
- Springel, V. & Hernquist, L., 2002, *MNRAS* **333**, 649
- Springel, V. & Hernquist, L., 2003a, *MNRAS* **339**, 289
- Springel, V. & Hernquist, L., 2003b, *MNRAS* **339**, 312
- Umemura, M., Loeb, A., & Turner, E. L., 1993, *ApJ* **419**, 459
- Valageas, P. & Silk, J., 1999, *A&A* **347**, 1
- Venkatesan, A., Giroux, M. L., & Shull, J. M., 2001, *ApJ* **563**, 1
- Volonteri, M., Haardt, F., & Madau, P., 2003, *ApJ* **582**, 559
- Volonteri, M., Madau, P., Quataert, E., & Rees, M. J., 2005, *ApJ* **620**, 69
- Volonteri, M. & Rees, M. J., 2005, *ApJ* **633**, 624
- Volonteri, M. & Rees, M. J., 2006, *ApJ* **650**, 669
- Wyithe, J. S. B. & Loeb, A., 2003, *ApJ* **586**, 693
- Yoo, J. & Miralda-Escudé, J., 2004, *ApJ* **614**, L25
- Yoshida, N., Abel, T., Hernquist, L., & Sugiyama, N., 2003, *ApJ* **592**, 645
- Zaroubi, S., Thomas, R. M., Sugiyama, N., & Silk, J., 2006, *astro-ph/0609151*

TABLE 1

OVERVIEW OF THE SIMULATION PARAMETERS OF THE MAIN RUNS. THE RUNS ARE LABELED WITH A LETTER INDICATING THE TYPE OF RUN, AND A NUMBER INDICATING THE MASS.

label	mass (M_{\odot}/h)	z_{vir}	λ	N (total, gas)	ϵ_f
A1	10^8	16	0.03	$10^6, 10^5$	0.05
A2	10^9	12	0.03	$10^6, 10^5$	0.05
A3	10^{10}	10	0.03	$10^6, 10^5$	0.05
A4	10^{11}	7.5	0.03	$5 \times 10^6, 5 \times 10^5$	0.05
B1	10^8	16	0.03	$10^6, 10^5$	0
B2	10^9	12	0.03	$10^6, 10^5$	0
B3	10^{10}	10	0.03	$10^6, 10^5$	0
B4	10^{11}	7.5	0.03	$5 \times 10^6, 5 \times 10^5$	0
C1	10^8	30	0.03	$10^6, 10^5$	0.05
C2	10^9	20	0.03	$10^6, 10^5$	0.05
C3	10^{10}	16	0.03	$10^6, 10^5$	0.05
C4	10^{11}	9	0.03	$10^6, 10^5$	0.05

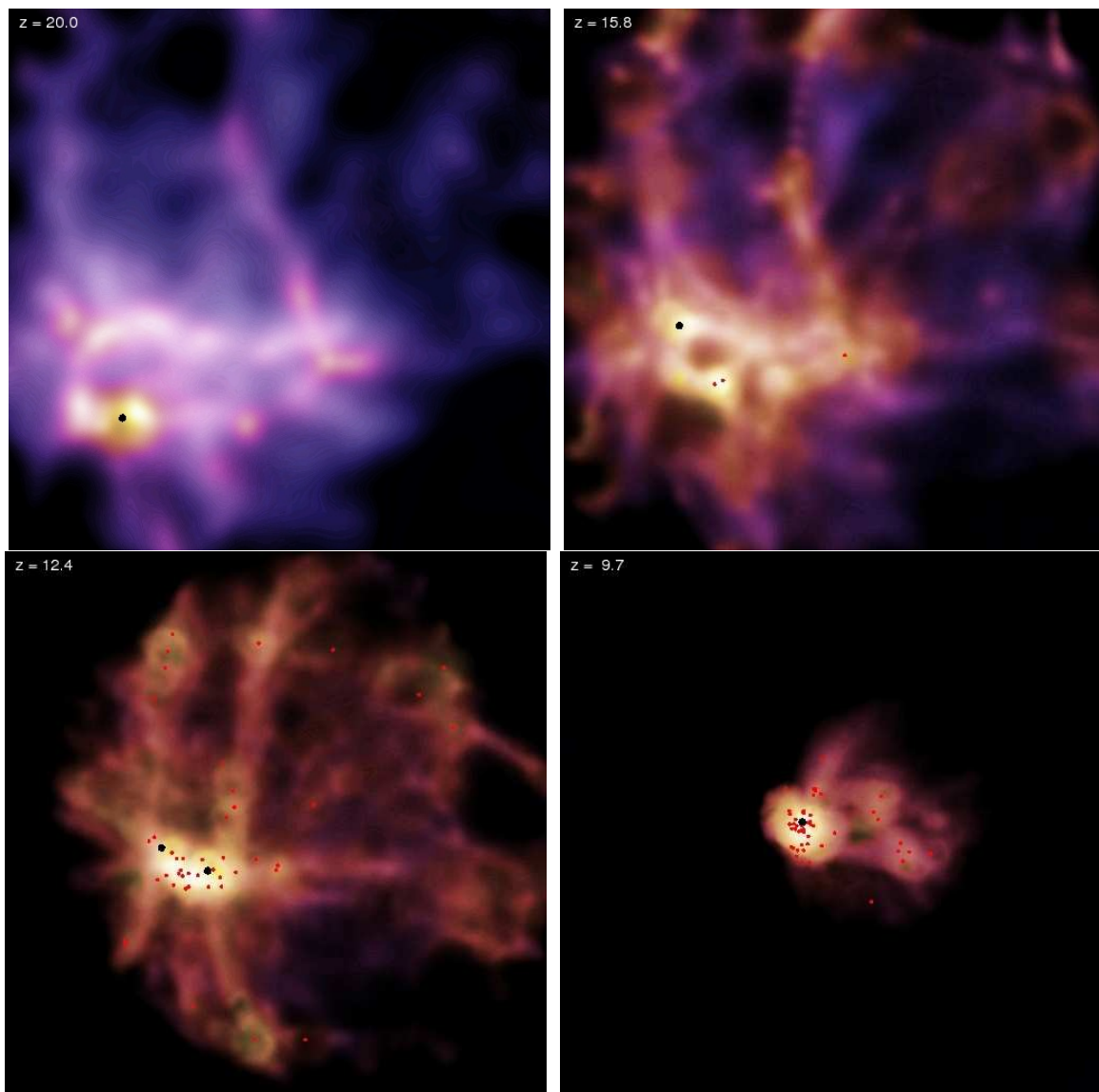


FIG. 1.— Evolution of gas density for a representative run. Shown is the gas density (indicated by brightness) color coded by temperature for the A3 run at (from top left to bottom right) redshifts of 20,15.7, 12.4 and 9.7. Width of the panels is 200 kpc (comoving). BH twice as massive as the seed are marked by red dots, the largest BH in each frame is enlarged and shown in black (for redshift 12 the two heaviest differ less than 20% in mass, and are both enlarged).

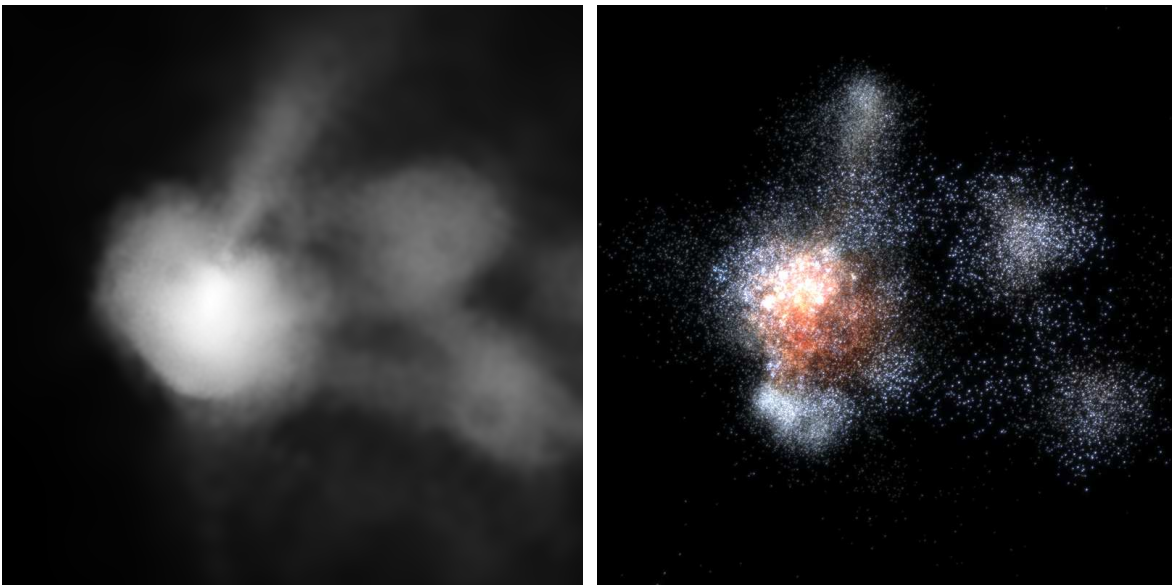


FIG. 2.— Projection of the gas distribution (top) and rest frame UVB composite rendering (bottom). Shown is a region 10 kpc wide of the A3 run at $z = 10$. The UVB panel includes stellar evolution and extinction by the ISM.

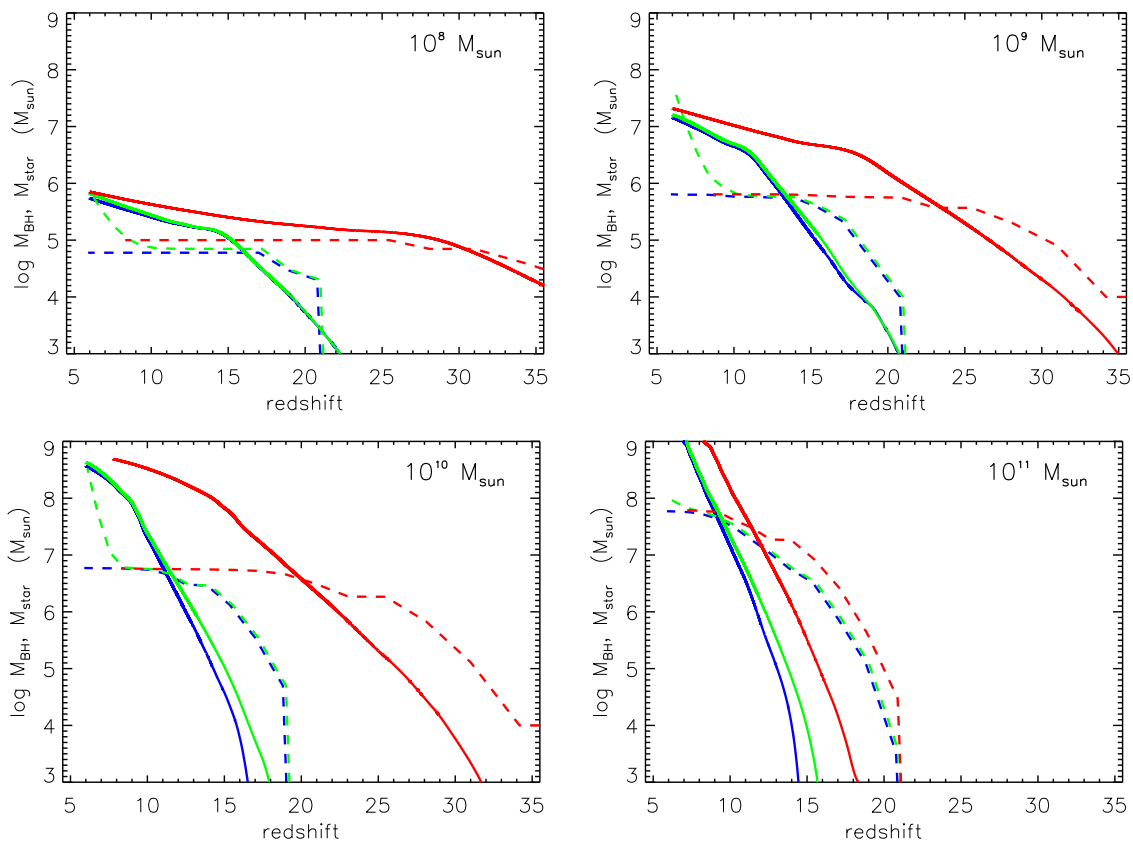


FIG. 3.— Evolution of the total stellar mass and black hole mass for the main simulations. Different panels show the results for halos of different mass (each panel labeled with the corresponding mass), the solid lines show the total stellar mass, the dashed lines show the total BH mass. Colors indicate the type of simulation: blue line=A (default), green line = B (no feedback) and red line = C (higher z collapse).

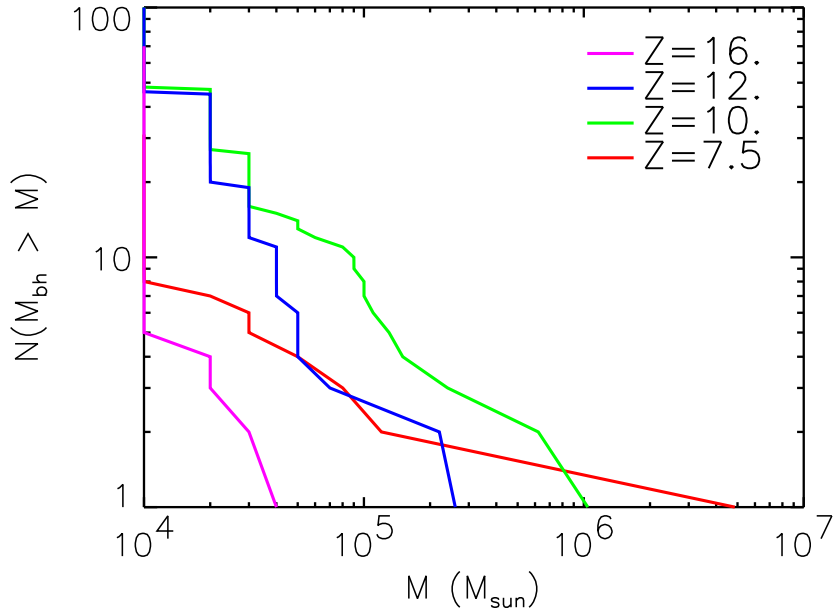


FIG. 4.— The evolution of the black hole mass function of the A3 run ($10^{10} M_{\odot}$). The plot shows the number of black holes $N(M_{\text{BH}} > M)$ per halo of the $10^{10} M_{\odot}$ A3 run as a function of mass for four different redshifts in the simulation.

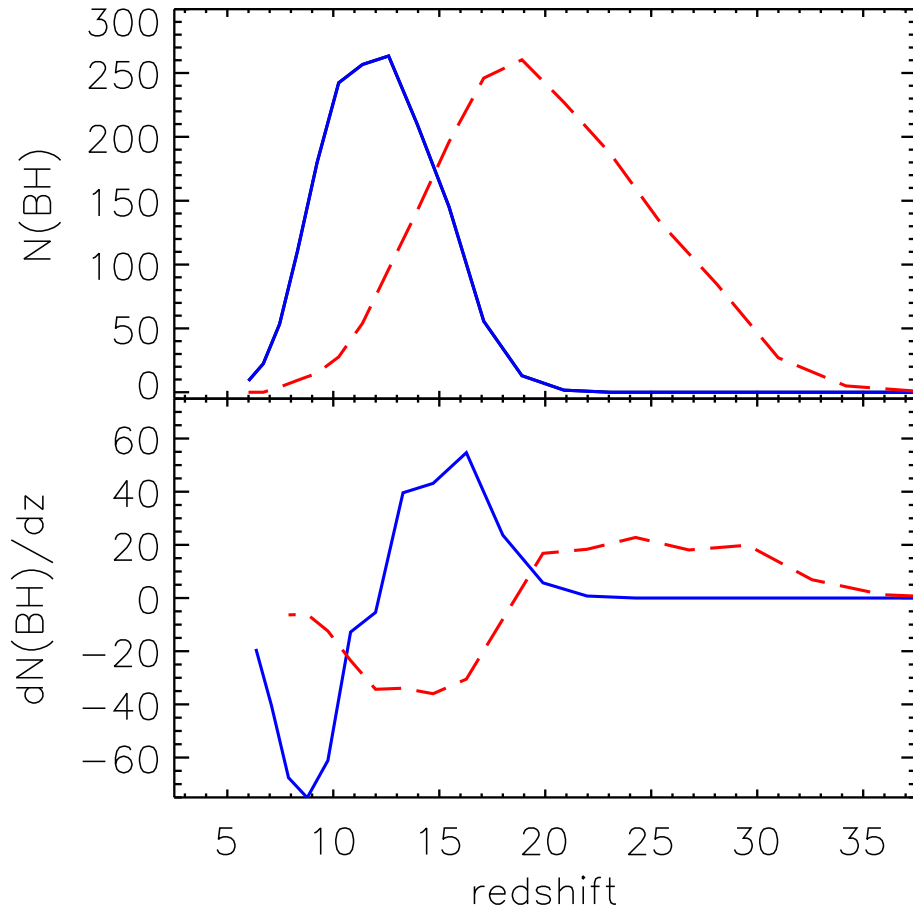


FIG. 5.— Black hole counts. top panel: total number of BH for the $10^{10} M_{\odot}$ runs as a function of redshift and bottom panel: BH formation rate. Blue drawn line shows results of the run A3 (normal z_{vir}), while the red dashed line is for the C3 run (high z_{vir}).

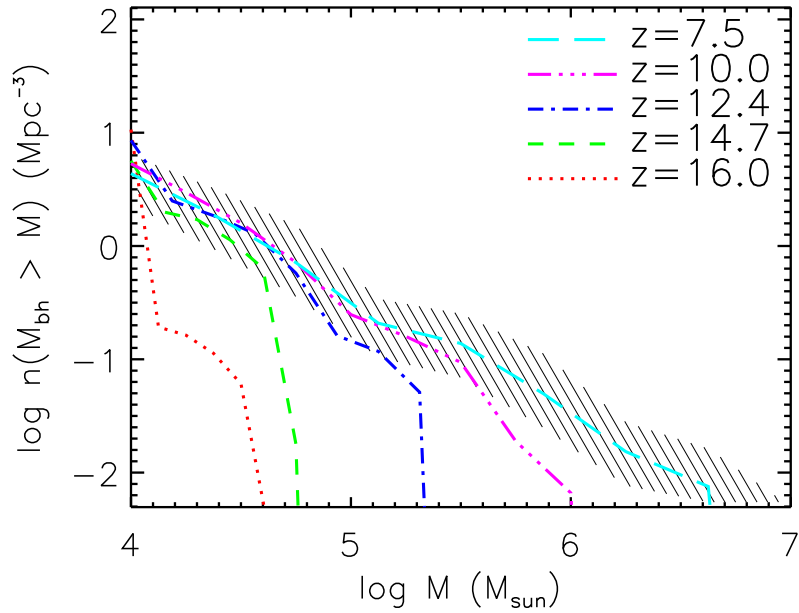


FIG. 6.— Global BH mass function at different redshift. Shown is the total mass function as derived from our simulations and the Press-Schechter formalism, for redshifts from 16 to 7.5. Shaded area gives the range of uncertainty from Poisson errors for $z = 7.5$. Similar ranges of uncertainty apply for the other redshifts, but are omitted for clarity.

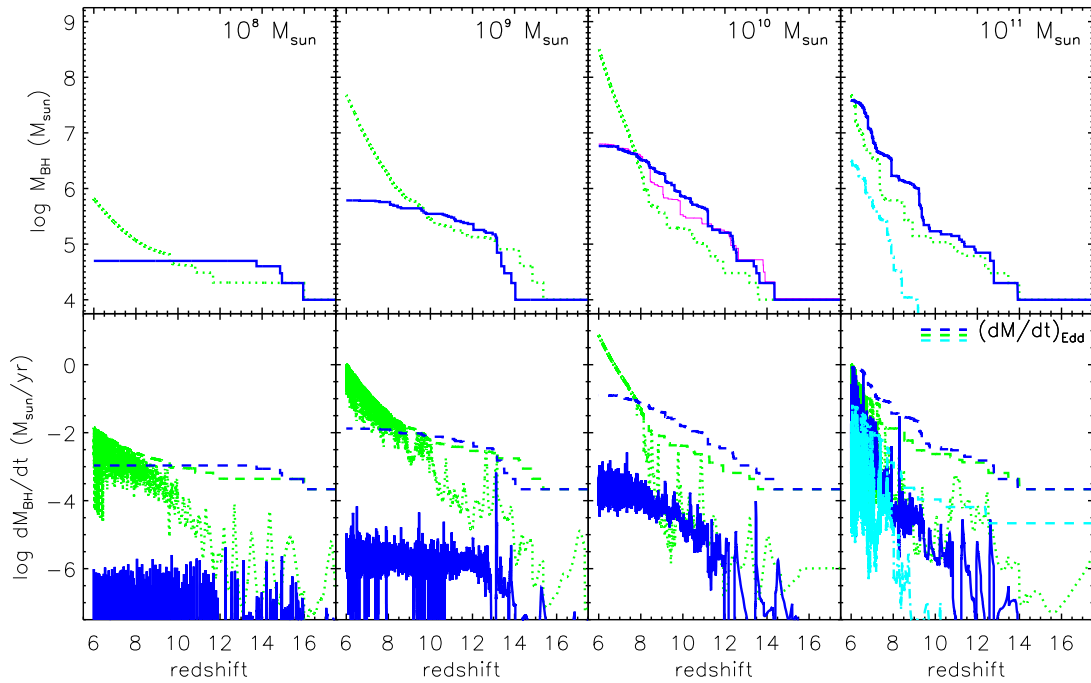


FIG. 7.— Mass and accretion rate of the central black hole for simulations of different halo mass and varying feedback strength. The mass of the parent halo is labeled in each panel. The top panels show the total mass as a function of redshift for the most massive black hole. Bottom panels show the corresponding accretion rates (drawn lines) as well as the Eddington accretion rates (dashed). In all panels, the blue line indicates simulations with a feedback strength of $\epsilon_f = 0.05$ (A runs), the green dotted lines those with $\epsilon_f = 0$ (B runs). An intermediate case for $\epsilon_f = 0.01$ is also shown (purple thin line) for the $10^{10} M_\odot$ simulation. The dash-dotted line in the $10^{11} M_\odot$ panel shows results for a reduced seed mass ($M_{\text{seed}} = 10^3 M_\odot$).

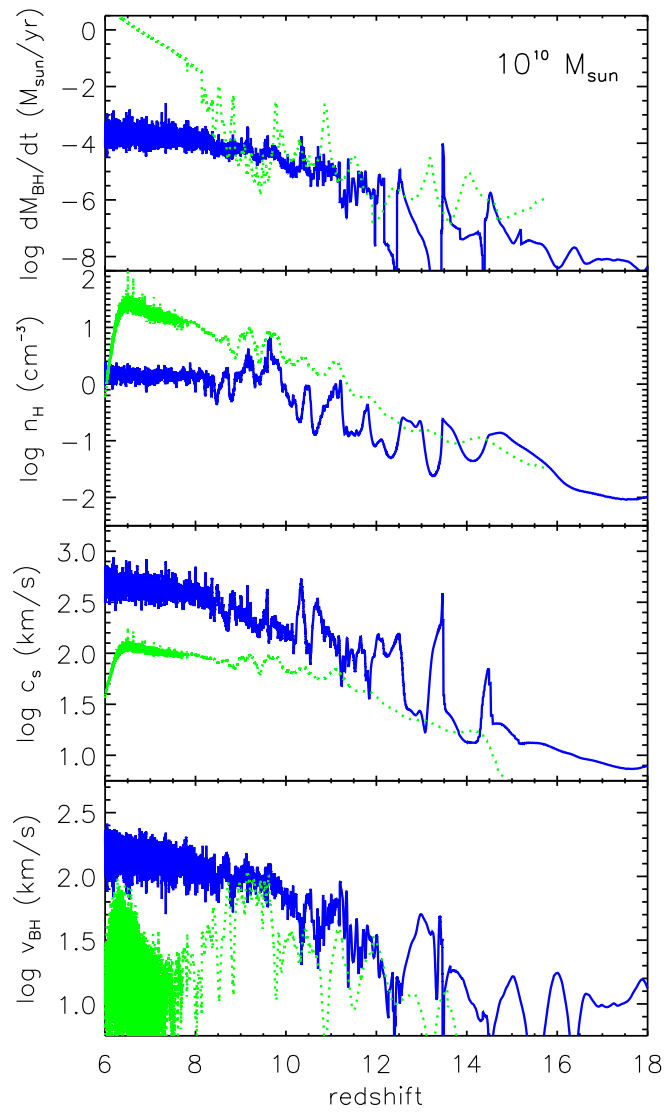


FIG. 8.— Evolution of the ISM properties around the BH. Plotted are (from top to bottom) BH accretion rate, local gas density, sound speed and the relative velocity of the BH with respect to the gas for the A3 (blue lines) and B3 (green dotted lines) runs.

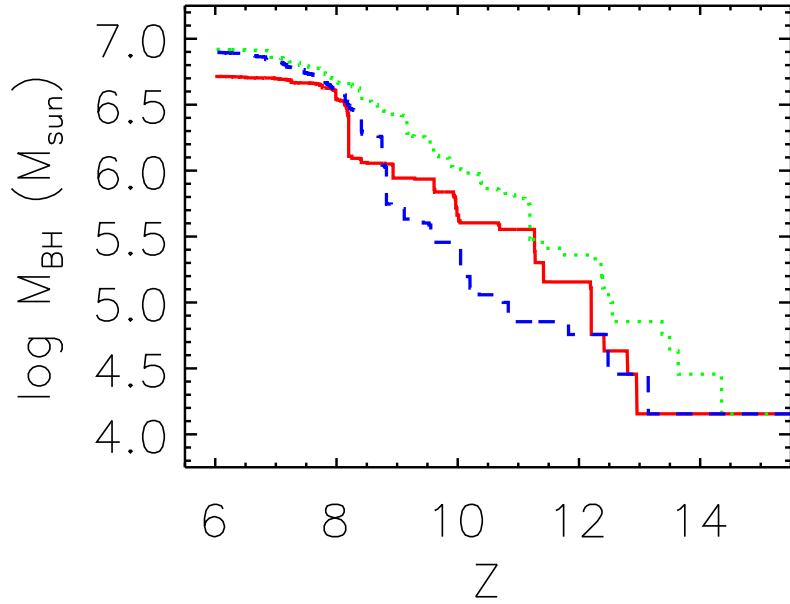


FIG. 9.— Resolution test for the $10^{10} M_{\odot}$ A3 run. Plotted is the mass of the most massive black hole in the simulation, for runs of different resolution, blue dashed line: (standard) $N = 10^6$, red drawn line: $N = 10^5$ and green dotted: $N = 5 \times 10^6$.

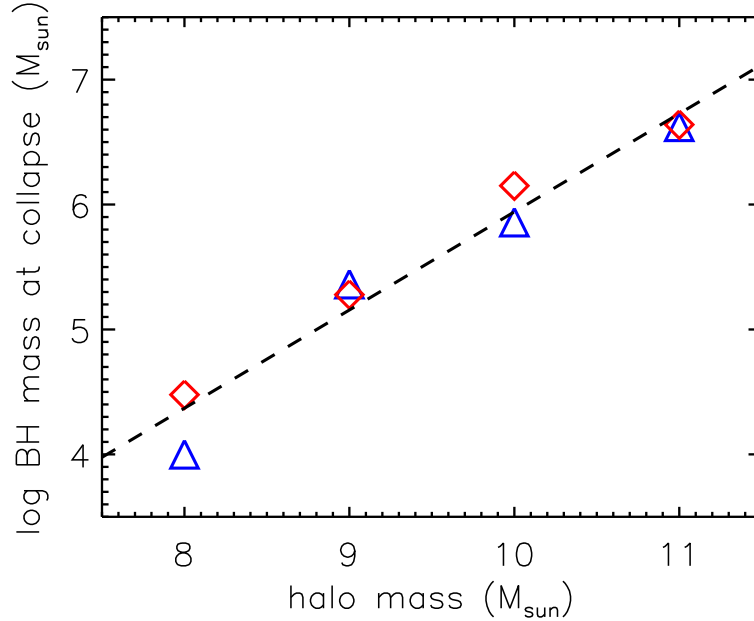


FIG. 10.— BH mass and halo mass. Plotted is the mass of the central most massive BH at the redshift of virialization of the parent halo as a function of halo mass. Blue triangles are the simulations of the “A” series (our default $3\text{-}\sigma$ runs), while the red diamonds are the “C” simulations (high collapse redshift). The dotted line is the fitted relation $M_{BH} = 5 \times 10^6 M_{\odot} (M_{halo} / 10^{11} M_{\odot})^{0.78}$.

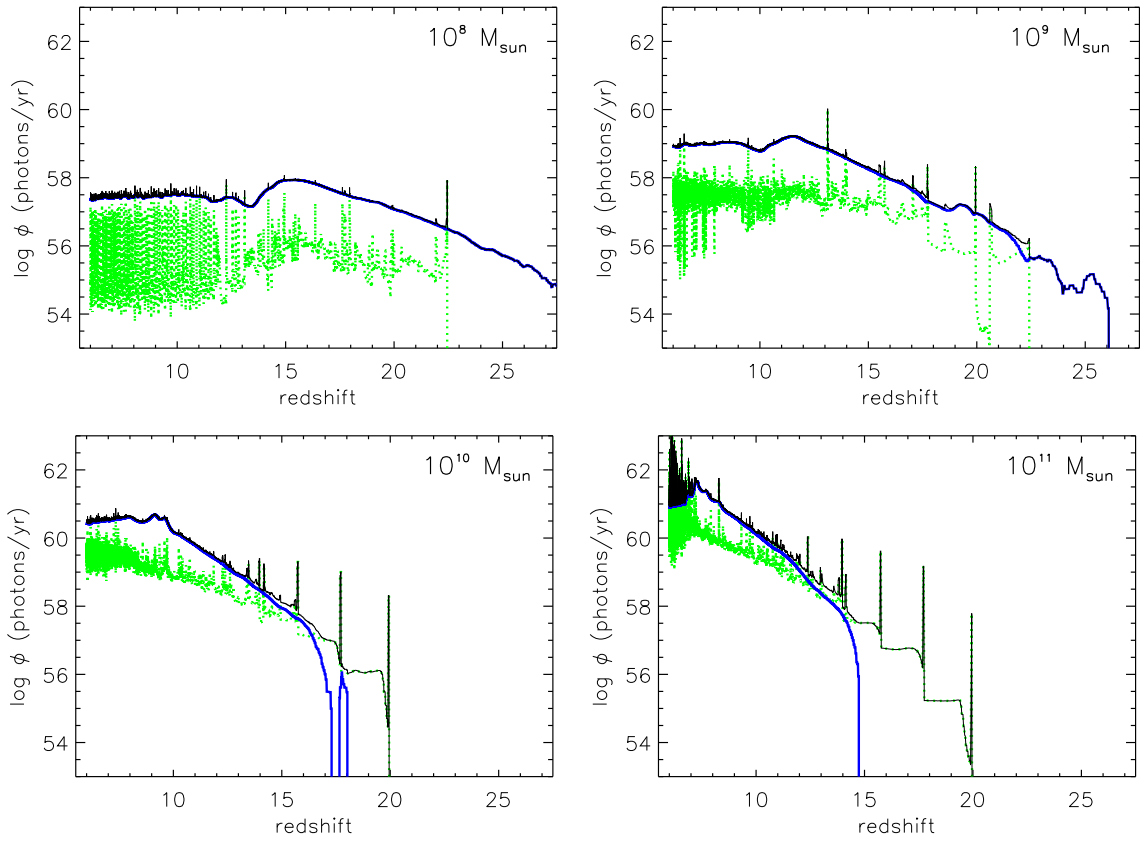


FIG. 11.— Ionizing photon production. Plotted are in blue drawn lines: the production rates ϕ_* of ionizing photons for the stars, in green dotted: ϕ_{BH} for the ionizing flux from all black holes and thin black drawn line: the total $\phi = \phi_* + \phi_{\text{BH}}$. For the stellar ionized photons it is assumed that photons are liberated instantaneously at the formation redshift.

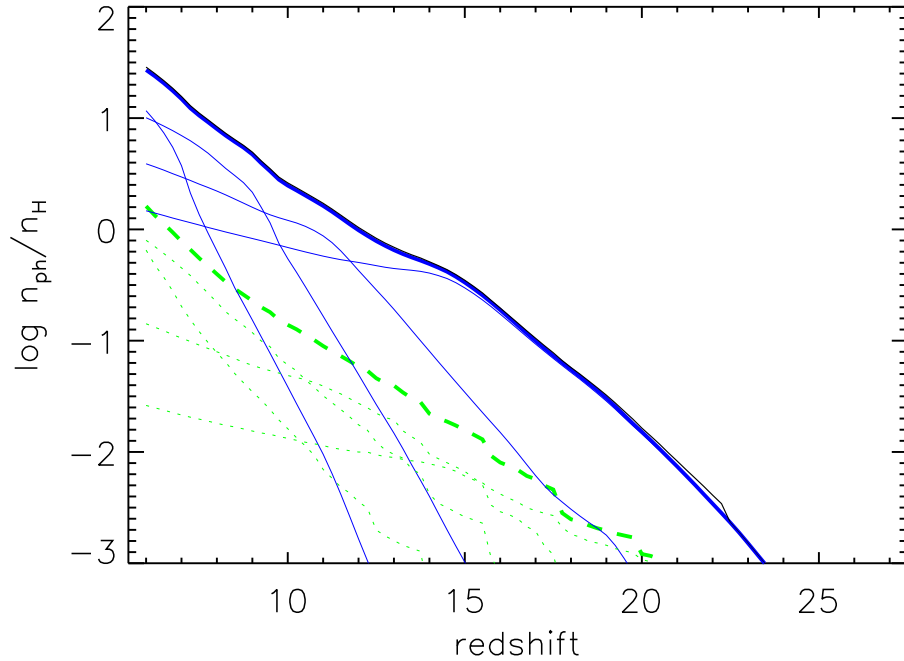


FIG. 12.— Cumulative number of ionizing photons per hydrogen atom. Plotted as a function of redshift in the blue drawn line: total number of ionized photons per hydrogen atom produced by stars $n_{\phi,*}/n_{\text{H}}$, in green dashed: $n_{\phi,\text{BH}}/n_{\text{H}}$ and thin black drawn line: $n_{\text{ph}}/n_{\text{H}} = (n_{\phi,*} + n_{\phi,\text{BH}})/n_{\text{H}}$. Drawn and dotted lines give the ‘contribution’ of the halos (A1-A4) of different masses towards the averaging procedure.

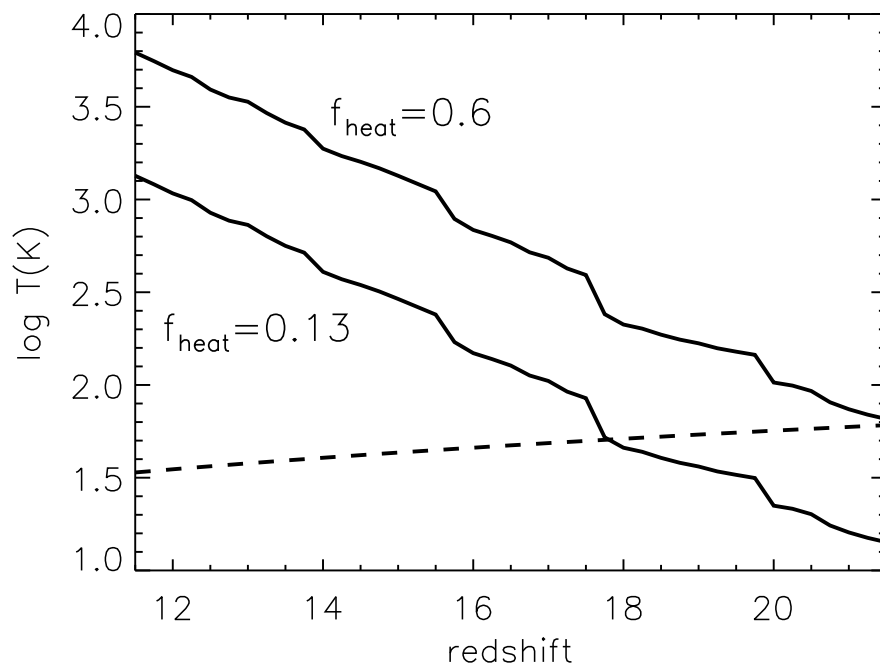


FIG. 13.— Temperature due to X-ray heating. Drawn lines give the temperatures of the IGM if heated by the X-rays generated from BH accretion (Eq. 7) as a function of redshift for two different values of the heating fraction, $f_{\text{heat}} = 0.13$ (appropriate for a low ionization fraction $x = 10^{-4}$) and $f_{\text{heat}} = 0.6$ ($x = 0.1$). Dashed line gives the CMB background temperature.